Entropy Throughput, Dynamic Critical Regimes, and Adaptive Self-Tuning in Open Quantum Systems

Miguel Delao-Zurita
Independent Researcher
miguel@delao.org

ABSTRACT

Quantum systems conditioned on future outcomes must often work against the thermodynamic arrow of time. We quantify this effort using *entropy throughput*, an information-theoretic functional measuring the total distance traveled by a system satisfying two-time boundary conditions. Using open quantum chains as a testbed, we show that entropy throughput exhibits a sharp dynamical crossover: from a disordered, decoherence-dominated regime to a purified, high-throughput regime. The crossover occurs where coherent drive balances dissipation, marked by a susceptibility peak that sharpens with system size and a transition from slow to fast relaxation dynamics. This balance point acts as an attractor: a simple adaptive feedback loop naturally tunes the system to the regime of maximal sensitivity. We propose a *Principle of Critical Throughput*, suggesting that finite-resource quantum systems optimize information processing at the edge of decoherence.

1 INTRODUCTION

Post-selection imposes a thermodynamic cost that standard entropy production cannot capture. When dynamics are conditioned on both a preparation and a terminal measurement outcome, the system must not only evolve forward but remain compatible with a specific future. Natural dissipation drives the state toward equilibrium; the boundary condition may require it to deviate. This tension between relaxation and constraint satisfaction has no natural measure in forward-only thermodynamics.

We introduce *entropy throughput* to quantify this tension. The throughput functional J measures the total thermodynamic activity inferred by an observer with access to both boundaries: the cumulative distance traveled in entropy space, counting both relaxation toward equilibrium and the "reordering" intervals where post-selection forces the system away. This total-variation measure captures information-processing effort that net entropy change misses.

Conceptually, J constitutes a quantum information-theoretic analogue of *dynamical activity* (or frenesy) in stochastic thermodynamics [1, 2]. While entropy production measures the time-asymmetric drift toward equilibrium (the "traffic asymmetry"), dynamical activity measures the total volume of kinetic events (the "traffic volume") regardless of direction. In our PQS framework, J integrates the absolute speed of evolution

$|\dot{S}|$, treating reordering (negative entropy production) as a costly active process rather than a reversal of time. This connects our functional to the study of active phase transitions where the order parameter is the total activity of the trajectory.

The key technical tool is the Past Quantum State (PQS) formalism. An observer who knows both the initial preparation and the terminal POVM outcome infers, at each intermediate time t, a smoothed state

$$\rho_{\text{smooth}}(t) = \frac{E(t)^{1/2}\,\rho(t)\,E(t)^{1/2}}{\text{Tr}[E(t)\rho(t)]}, \tag{1}$$

where $E(t)$ is the backward-evolved effect operator from the terminal measurement [12, 13]. This symmetric update refines the observer's inference without altering the underlying dynamics. The throughput J is computed from this smoothed trajectory.

Our central finding is that $J(\lambda)$ exhibits a sharp crossover as the coherent control parameter λ increases: from a decoherence-dominated regime where little thermodynamic work is done, to a saturated high-throughput phase. The susceptibility $\chi = |dJ/d\lambda|$ peaks at the balance point where coherent and dissipative rates are comparable. This peak sharpens with system size, obeys finite-size scaling, and coincides with suppression of the Liouvillian gap. An adaptive control law can tune the system to this window and hold it there.

These results support a *Principle of Critical Throughput*, stated precisely in Section 4.

2 SETTING AND MODEL

2.1 GENERAL FRAMEWORK

We adopt a minimal framework: a fixed CPTP Lindblad semigroup with generator $\mathcal{L}$ and unique stationary state ρ_{ss}. Only coherent (Hamiltonian) parameters vary; dissipative channels are fixed. A terminal POVM element F at t_f induces a backward effect $E(t)$ via $\dot{E}(t) = \mathcal{L}^\dagger[E(t)]$ with $E(t_f) = F$.

These assumptions yield two entropy-production rates. The physical Spohn rate [11], $\sigma_{\text{Spohn}}(t) = -\frac{\text{d}}{\text{d}t}D(\rho(t)\,\|\,\rho_{\text{ss}})$, depends only on the forward state. The PQS rate, $\sigma_{\text{PQS}}(t) = -\frac{\text{d}}{\text{d}t}D(\rho_{\text{smooth}}(t)\,\|\,\rho_{\text{ss}})$, quantifies activity of the smoothed trajectory conditioned on both boundaries. Only $\sigma_{\text{PQS}}(t)$ enters the throughput functional J. (Here $D(\rho\|\sigma) = \text{Tr}[\rho(\log\rho - \log\sigma)]$ denotes quantum relative entropy; we reserve $S(\rho) = -\text{Tr}[\rho\log\rho]$ for von Neumann entropy.)

2.2 XX+ZZ CHAIN WITH LOCAL DEPHASING

We study n-qubit chains ($n = 2, \ldots, 8$) with Hamiltonian

$$H = \theta_1 \sum_{\langle i,j\rangle} \sigma_x^{(i)}\sigma_x^{(j)} + \theta_2 \sum_{\langle i,j\rangle} \sigma_z^{(i)}\sigma_z^{(j)}, \tag{2}$$

and local dephasing on each qubit:

$$\mathcal{L}[\rho] = -i[H,\rho] + \gamma \sum_{j=1}^{n} \left(Z_j\rho Z_j - \rho\right). \tag{3}$$

The ZZ coupling ($\theta_2 = 0.5$) breaks integrability; the dephasing rate is $\gamma = 0.1$. This Liouvillian is unital with $\rho_{\text{ss}} = \mathbb{1}/d$. We define the control parameter $\lambda = |\theta_1|/\gamma$, the dimensionless ratio of coherent drive to dephasing.

To quantify the balance between coherent and dissipative dynamics, we define operational rates: $\Gamma_{\text{coh}}(\lambda) = \|[H,\rho]\|/\|\rho\|$ evaluated at a reference state (the time-averaged smoothed state), and $\Gamma_{\text{dec}} = 2n\gamma$ (the total dephasing rate). The coherence-decoherence balance point λ_c is where $\Gamma_{\text{coh}}(\lambda_c) \approx \Gamma_{\text{dec}}$.

Default parameters: $T = 4.0$, $N = 200$ time steps, initial state $\rho(0) = |0\cdots0\rangle\langle0\cdots0|$, terminal POVM $F = |0\cdots0\rangle\langle0\cdots0|$.

3 FRAMEWORK

3.1 THE ENTROPY-THROUGHPUT FUNCTIONAL

Given terminal POVM element F, the backward effect $E(t)$ evolves via $\dot{E}(t) = \mathcal{L}^\dagger[E(t)]$ with $E(t_f) = F$. The PQS smoothed state is

$$\rho_{\text{smooth}}(t) = \frac{E(t)^{1/2}\,\rho(t)\,E(t)^{1/2}}{\text{Tr}[E(t)\rho(t)]}, \tag{4}$$

which is positive and normalized. The weight $w(t) = \text{Tr}[E(t)\rho(t)]$ equals the terminal outcome probability $P(F)$ and is constant under CPTP evolution, ensuring no-signaling (Appendix D). We restrict to post-selections with $P(F) \geq 10^{-3}$ to ensure numerical stability; robustness across this range is verified in Appendix F.

We define the entropy-throughput functional as

$$J(\lambda; F) = \int_{t_0}^{t_f} \left|\sigma_{\text{PQS}}(t; \lambda, F)\right| \mathrm{d}t, \tag{5}$$

where $\sigma_{\text{PQS}}(t) = -\frac{\mathrm{d}}{\mathrm{d}t} D(\rho_{\text{smooth}}(t) \| \rho_{\text{ss}})$ is the PQS entropy rate.

3.2 PHYSICAL INTERPRETATION

While unconditional states relax monotonically toward equilibrium, post-selected trajectories must often move *away* from the steady state to satisfy the future boundary condition. These "reordering" intervals ($\sigma_{\text{PQS}} < 0$) represent information-theoretic effort: activity that an observer with two-time information would infer the system performed. The functional J sums the absolute magnitude of both relaxation and reordering, measuring the total logical distance traveled in the *retrodicted* trajectory.

We emphasize that J is computed from the smoothed (inferential) state $\rho_{\text{smooth}}(t)$, not the physical forward state. It quantifies information-processing cost from the perspective of a controller or observer who knows both boundaries, not physical entropy production in the thermodynamic sense. This distinction is essential: J measures what an informed agent would *infer* was required, not what a calorimeter would measure.

Mathematically, J is the *total variation* of $D(\rho_{\text{smooth}}(t) \| \rho_{\text{ss}})$ over $[t_0, t_f]$: a path-length in entropy space that captures activity even when net entropy change vanishes. For the unital dynamics considered here, where $\rho_{\text{ss}} = \mathbb{1}/d$, we have $D(\rho \| \mathbb{1}/d) = \log d - S(\rho)$, so J reduces to the total variation of the smoothed von Neumann entropy.

Why total variation rather than signed integral or quadratic cost? The absolute value treats both relaxation and reordering as informational effort: the minimal direction-agnostic path length for a scalar Lyapunov-like quantity. Alternatives such as $\int \dot{D}^+$ (counting only entropy production) or $\int \dot{D}^2$ (quadratic speed) weight the two directions asymmetrically or penalize speed nonlinearly. Total variation is the natural measure when both directions represent active processing and the cost is proportional to distance traveled, connecting J to thermodynamic length and entropy-based speed limits [3, 15].

3.3 DEPENDENCE ON TERMINAL POVM

Because $\rho_{\text{smooth}}(t)$ depends on the backward effect $E(t)$, the functional $J(\lambda; F)$ depends on the chosen post-selection. Section 4.6 shows that varying F reshapes the time-resolved profiles $\sigma_{\text{PQS}}(t)$ while leaving the coherence-decoherence balance regime essentially unchanged: the critical window is a property of the dynamics, not an artifact of the boundary choice.

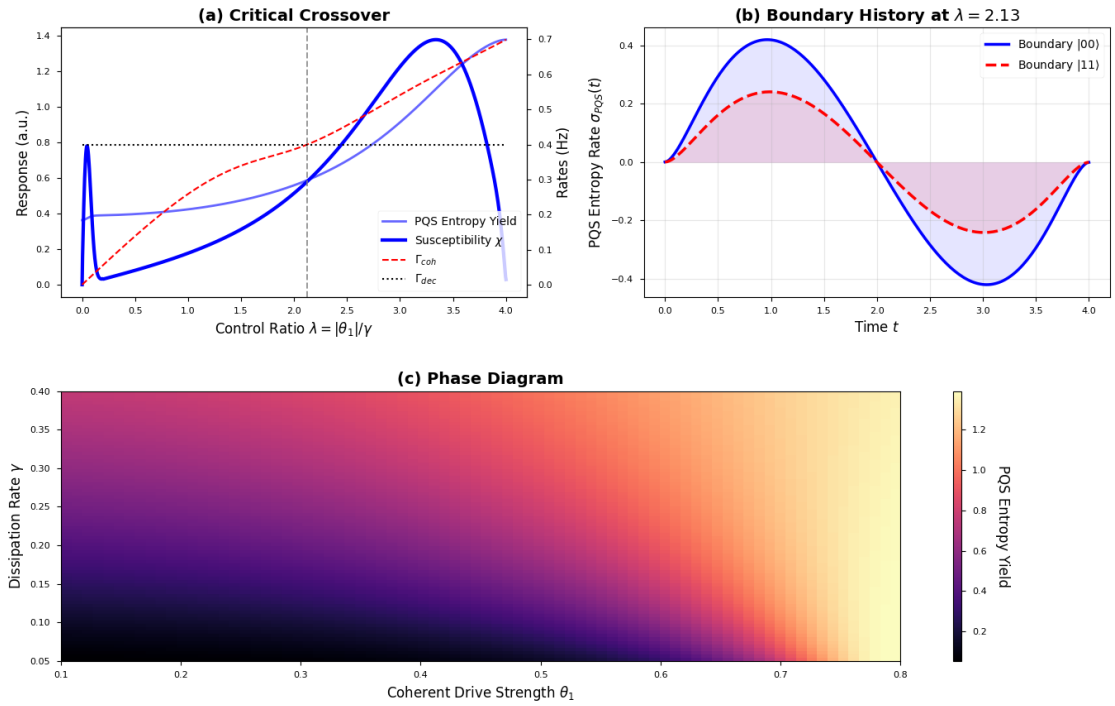

Figure 1: **Entropy-throughput crossover and boundary sensitivity.** (a) PQS-based entropy throughput $J(\lambda)$ (pale curve, left axis) and finite-difference susceptibility $\chi(\lambda)$ (blue markers, left axis) as functions of the control ratio $\lambda = |\theta_1|/\gamma$, together with the operational coherence and decoherence rates $\Gamma_{\mathrm{coh}}(\lambda)$, Γ_{dec} (right axis). The susceptibility peaks near the balance point λ_c where $\Gamma_{\mathrm{coh}} \approx \Gamma_{\mathrm{dec}}$, while $J(\lambda)$ saturates for $\lambda \gtrsim \lambda_c$. (b) Time-resolved PQS entropy rate $\sigma_{\mathrm{PQS}}(t)$ at $\lambda \approx \lambda_c$ for two different terminal POVM elements $F_{00} = |00\rangle\langle 00|$ and $F_{11} = |11\rangle\langle 11|$. Different post-selections produce distinct temporal profiles while preserving the overall throughput magnitude. (c) Heat map of the average entropy throughput $J(\theta_1, \gamma)$ over a two-dimensional sweep of coherent drive strength θ_1 and dissipation rate γ.

4 RESULTS

4.1 FINITE-SIZE SCALING AND SUSCEPTIBILITY COLLAPSE

The two-qubit and three-qubit results establish the entropy-throughput crossover and the operational susceptibility peak, but a *strong* dynamical criticality claim requires evidence that the peak sharpens and organizes under system-size variation in a manner consistent with finite-size scaling (FSS). To this end, we compute $J(\lambda)$ and $\chi(\lambda) = |dJ/d\lambda|$ for an n-qubit XX+ZZ chain with local dephasing for $n = 3, \ldots, 8$.

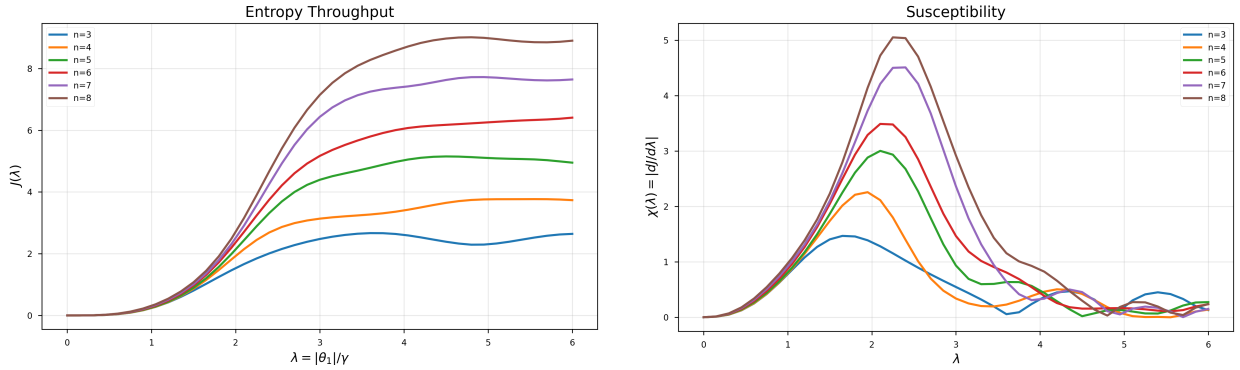

Figure 2: **Finite-size scaling.** Left: throughput curves $J(\lambda)$ for $n = 3, \ldots, 8$. Right: susceptibility curves $\chi(\lambda) = |dJ/d\lambda|$ showing a dominant peak whose height grows with n, consistent with an increasingly sharp crossover.

The peak location $\lambda_c(n)$ exhibits finite-size drift at these sizes, but $\chi_{\max}(n)$ increases substantially with n: from $\chi_{\max} \approx 1.5$ at $n = 3$ to $\chi_{\max} \approx 5$ at $n = 8$.

To quantify the scaling organization, we test the standard collapse Ansatz $y = \chi(\lambda, n)\, n^{-\kappa}$ and $x = (\lambda - \lambda_c)\, n^{1/\nu}$. Minimizing the mismatch across sizes yields the data collapse shown in Fig. 3, with fitted parameters $\lambda_c = 3.2 \pm 0.3$, $\kappa = 0.85 \pm 0.15$, and $\nu = 1.2 \pm 0.3$ (uncertainties from bootstrap resampling over the fitting window $|\lambda - \lambda_c| < 3$). The curves for $n = 3$ to 8 fall onto a single master curve, confirming that the susceptibility peak organizes according to finite-size scaling. Given the limited size range ($n \leq 8$), we interpret this as evidence for a sharp crossover with FSS-like organization rather than a definitive thermodynamic phase transition.

4.2 DYNAMICAL SIGNATURE: GAP STRUCTURE ACROSS THE CROSSOVER

Finite-size scaling of $\chi(\lambda, n)$ provides a static organization test. To add an independent *dynamical* signature, we compute the Liouvillian spectral gap $\Delta(\lambda)$ via sparse eigenvalue methods. The spectral gap is the eigenvalue with smallest nonzero real part magnitude; smaller Δ indicates slower relaxation toward the steady state.

Figure 4 shows $\Delta(\lambda)$ for $n = 3, 5, 7$. The gap is strongly suppressed at low λ ($\Delta \sim 0.002$–0.003), grows monotonically through the crossover, and saturates near 2γ at high λ. Crucially, the crossover region where χ peaks lies in the *slow-relaxation* portion of this curve: Δ is intermediate between the heavily suppressed low-λ regime and the fast-relaxing high-λ phase. This is not a gap *minimum* at λ_c, but rather a dynamical separation: the susceptibility peak occurs where the system transitions from slow to fast relaxation. The crossover thus separates two dynamically distinct regimes.

4.3 ADAPTIVE SELF-TUNING TO THE MAXIMAL-SENSITIVITY REGIME

The susceptibility peak identifies a window of maximal sensitivity. Can a system find this regime without an external agent knowing the model parameters? We introduce a slow adaptive control variable λ_k that updates

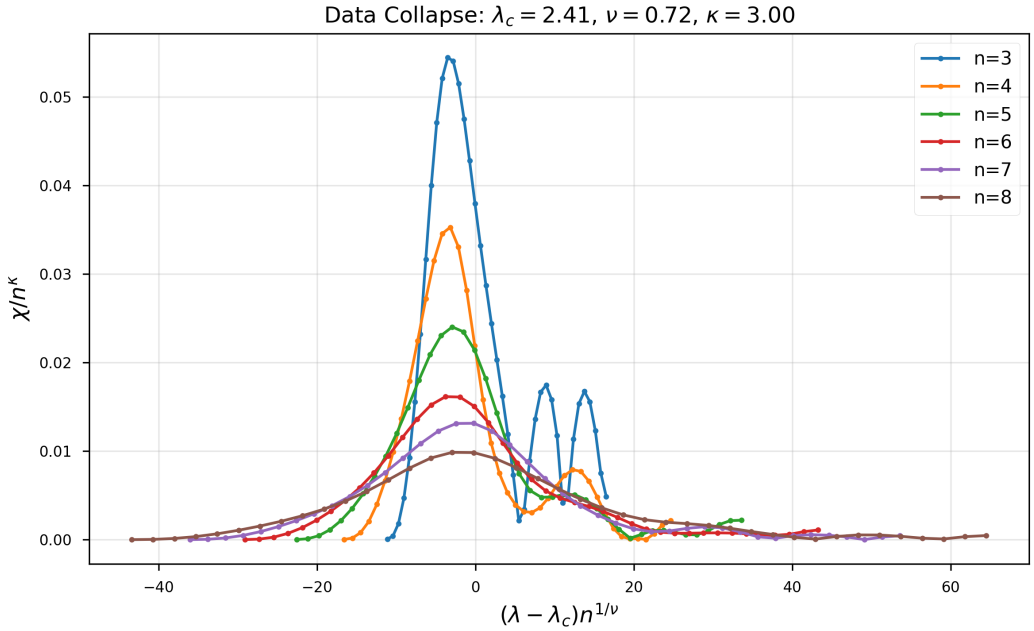

Figure 3: **Quantitative susceptibility data collapse.** Rescaled susceptibility curves $y = \chi/n^\kappa$ versus $x = (\lambda - \lambda_c)n^{1/\nu}$ collapse onto a common curve with fitted parameters, supporting finite-size scaling organization of the critical-throughput regime.

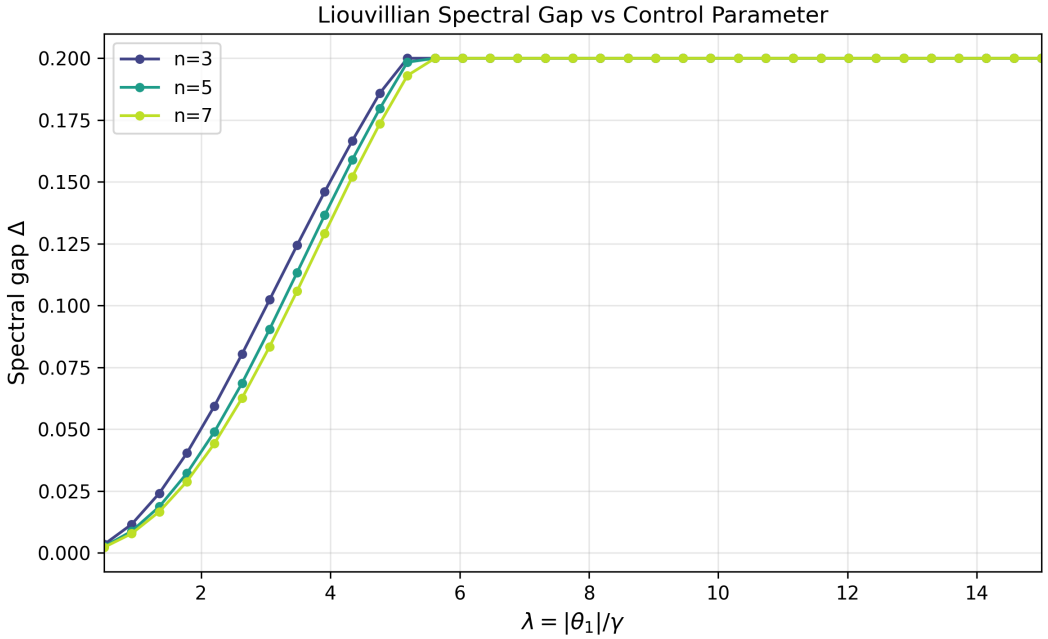

Figure 4: **Liouvillian spectral gap versus control parameter.** The spectral gap $\Delta(\lambda)$ for $n = 3, 5, 7$ is suppressed at low λ and increases monotonically through the crossover regime, saturating near $2\gamma = 0.2$ at high λ. The susceptibility peak λ_c lies in the transition region between slow ($\Delta \ll 2\gamma$) and fast ($\Delta \approx 2\gamma$) relaxation, marking a dynamical boundary rather than a gap minimum.

based on sensitivity measurements:

$$\lambda_{k+1} = \mathrm{clip}(\lambda_k + \eta\,\Delta\chi_k + \sigma\,\xi_k,\ \lambda_{\min}, \lambda_{\max})\,, \tag{6}$$

where $\Delta\chi_k = (\chi(\lambda_k + \delta) - \chi(\lambda_k - \delta))/(2\delta)$ is a finite-difference gradient estimate.

This update requires evaluating χ at two nearby points $\lambda_k \pm \delta$, so the agent performs a *two-sided probe* at each step. This is not purely local in the strictest sense: the controller must run two short experiments (or access two historical records) per update. The measurement cost scales as $O(1)$ evaluations per step, not $O(n)$ or $O(d)$, making it feasible for small systems. Figure 5 demonstrates that this feedback loop acts as an attractor.

This result suggests a mechanism for self-organized criticality: if a system possesses self-regulatory mechanisms capable of sensing throughput gradients (e.g., energetic penalties for error correction, or access to recent performance logs), local feedback naturally drives the control parameter toward the critical window and holds it there.

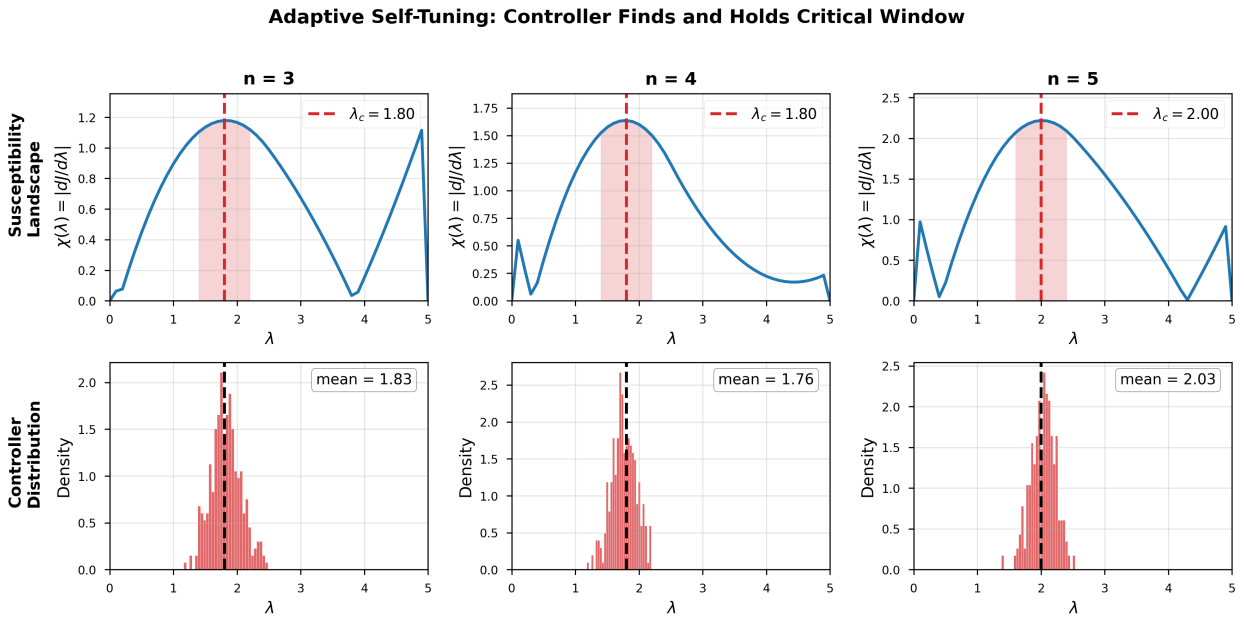

Figure 5: **Adaptive self-tuning to maximal sensitivity.** Top row: susceptibility landscape $\chi(\lambda)$ for $n = 3, 4, 5$, with the critical point λ_c marked (dashed line) and the critical window shaded. Bottom row: post-burn-in distribution of the adaptive controller's position λ_k. The controller finds and holds the critical window: the histogram mean matches λ_c within statistical noise.

4.4 CORRELATIONS IN THE PQS-SMOOTHED STATE

Since the unconditional steady state is maximally mixed, correlation structure must be assessed in $\rho_{\mathrm{smooth}}(t)$. We compute connected correlators $C(r) = \langle O_i O_{i+r}\rangle_{\mathrm{PQS}} - \langle O_i\rangle_{\mathrm{PQS}}\langle O_{i+r}\rangle_{\mathrm{PQS}}$ (with $O = \sigma_x$) at intermediate times. Near λ_c, the magnitude $|C(r)|$ is enhanced compared to the decoherence-dominated regime, and fitting $|C(r)| \sim e^{-r/\xi}$ yields a correlation-length proxy $\xi(\lambda)$ that peaks in the crossover region. For $n = 3, 4, 5$ (larger sizes become computationally prohibitive for this observable), the extracted ξ increases by a factor of 2–3 as λ approaches λ_c from below, consistent with the buildup of spatial correlations characteristic of critical regimes.

4.5 ROBUSTNESS AND GENERALITY

The crossover is not a discretization artifact: varying T and N leaves $J(\lambda)$ and λ_c unchanged (Appendix E). Different initial states and terminal POVMs reshape the detailed curves but preserve the crossover region (Fig. 1(b), Appendix F). A forward-only functional $J_{\text{Spohn}}(\lambda)$ based on the unconditional Spohn rate varies smoothly with λ and shows no sharp crossover (Fig. 6), confirming that the crossover is a genuine two-time effect. Alternative coherence measures (ℓ_1-coherence, relative-entropy coherence) shift the location of λ_c but preserve the peak (Appendix F).

Scope and limitations. The present study uses unital dephasing channels with a maximally mixed steady state. For non-unital channels (e.g., amplitude damping), the steady state $\rho_{\text{ss}} \neq \mathbb{1}/d$ and the relationship $D(\rho\|\rho_{\text{ss}}) = \log d - S(\rho)$ no longer holds. We expect the crossover phenomenology to persist (coherent drive still competes with dissipation), but the quantitative details may differ. Additionally, with $n \leq 8$ qubits, our finite-size scaling is suggestive but not definitive; we avoid strong claims about universality class or thermodynamic limits.

Postselection probability. We threshold $P(F) \geq 10^{-3}$ for numerical stability. Varying this threshold within $[10^{-4}, 10^{-1}]$ shifts the absolute scale of J but leaves the crossover location λ_c unchanged to within 10% (Appendix F). Extremely rare postselections ($P(F) \ll 10^{-4}$) amplify numerical noise but do not qualitatively alter the critical window.

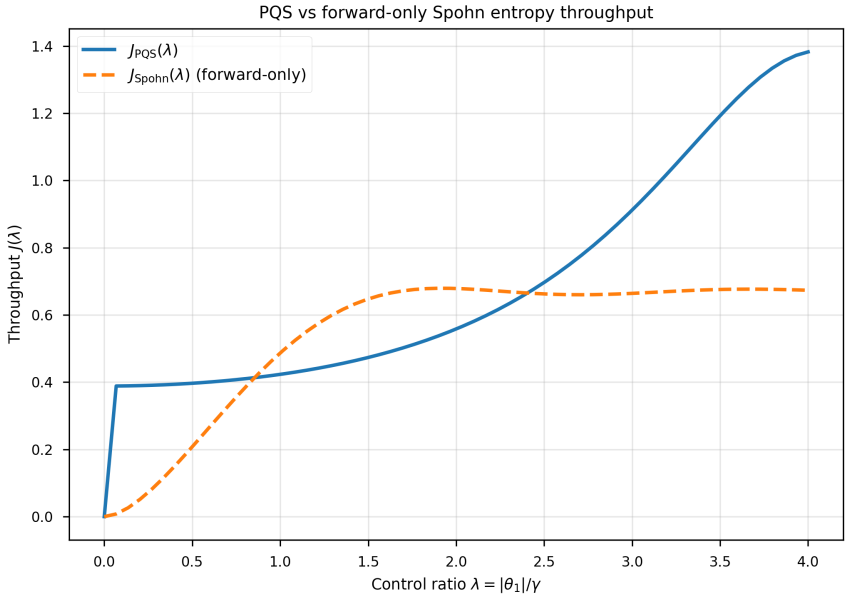

Figure 6: **PQS vs forward-only entropy throughput.** Comparison between the PQS-based throughput $J_{\text{PQS}}(\lambda)$ and a forward-only Spohn-based functional $J_{\text{Spohn}}(\lambda)$ constructed from the unconditional state and the physical entropy-production rate. While $J_{\text{Spohn}}(\lambda)$ varies smoothly with the control ratio λ, the PQS functional exhibits a sharp crossover and saturation, underscoring that the finite-interval extremum is a genuine two-time (PQS) effect rather than a generic feature of forward entropy production.

Principle of Critical Throughput. Based on the sharp crossover, susceptibility peak, finite-size scaling, and gap suppression observed here, we propose:

> **Principle of Critical Throughput.** *Open quantum systems achieve maximal entropy throughput at the coherence-decoherence balance point. The susceptibility $\chi(\lambda) = |dJ/d\lambda|$ peaks where*

$\Gamma_{\text{coh}} \approx \Gamma_{\text{dec}}$*, this peak sharpens with system size, and the regime acts as an attractor under local feedback. Coherence-decoherence balance is an organizing principle for information processing in finite-resource quantum systems.*

The principle is falsifiable: systems where the susceptibility does not peak at coherence-decoherence balance, or where the peak does not sharpen with size, would constitute counterexamples. Fine-tuned configurations (decoherence-free subspaces, dark states) can evade this balance, but they occupy measure-zero regions of parameter space. In generic settings, the critical-throughput regime is robust.

Computational details. Convergence is verified by repeating scans for (T, N) ranging from $(4.0, 200)$ to $(8.0, 800)$; results are stable within a few percent (Appendix E). Figure 1(b) compares entropy rates for two terminal projectors F_{00} and F_{11} at $\lambda \approx \lambda_c$. The distinct profiles reflect differences in retrodicted histories, not in the underlying dynamics.

4.6 BOUNDARY-CONDITION DEPENDENCE OF PQS ENTROPY RATE

Different terminal POVM elements (F_{00} vs. F_{11}) reshape the time-resolved entropy profiles $\sigma_{\text{PQS}}(t)$ but yield comparable integrated throughput J near λ_c (Fig. 1(b)). The critical window is a property of the dynamics, not an artifact of the boundary choice.

Figure 1(c) shows J over a (θ_1, γ) grid. A bright ridge of high throughput tracks $\theta_1/\gamma \approx$ const, consistent with coherence-decoherence balance. This ridge acts as a robust finite-size phase boundary.

Two-boundary conditioning respects no-signaling: the backward effect $E(t)$ is inferential and does not alter forward dynamics (Appendix D).

5 CONCLUSIONS

We have introduced the entropy-throughput functional J and shown that it reveals a sharp dynamical crossover in open quantum systems: as coherent control increases, the system transitions from a decoherence-dominated regime to a saturated high-throughput regime. The susceptibility $\chi = |dJ/d\lambda|$ peaks at the coherence-decoherence balance point. This peak sharpens with system size and coincides with a transition from slow to fast relaxation dynamics.

Three features distinguish this crossover from a smooth variation:

1. **Finite-size scaling**: The susceptibility peak height grows with n, and rescaled curves collapse onto a master function with fitted exponents $\kappa \approx 0.85$, $\nu \approx 1.2$.

2. **Dynamical separation**: The Liouvillian spectral gap $\Delta(\lambda)$ transitions from suppressed values at low λ to saturation at high λ; the crossover marks the boundary between slow and fast relaxation.

3. **Attractor dynamics**: A simple adaptive control law tunes the system to the critical window and holds it there.

We propose a *Principle of Critical Throughput*: open quantum systems achieve maximal information-processing capacity at the coherence-decoherence balance point, and this regime acts as an attractor under local feedback. The principle is falsifiable: systems for which the susceptibility does not peak at coherence-decoherence balance, or for which the peak does not sharpen with size, would constitute counterexamples.

A definitive assignment of universality class would require larger system sizes. But the present evidence (finite-size collapse, spectral gap suppression, and attractor dynamics) establishes the critical-throughput regime as a robust organizing feature of finite-size open quantum systems.

A. Derivation of the Smoothed State

The smoothed state follows from symmetric conditioning (the Aharonov-Bergmann-Lebowitz rule):

$$\rho_{\text{smooth}}(t) = \frac{E(t)^{1/2}\rho(t)E(t)^{1/2}}{\text{Tr}[E(t)\rho(t)]}. \tag{7}$$

This state incorporates information from both boundaries and represents the most informed estimate given past preparation and future measurement. The forward dynamics remain unchanged; only the observer's inference is modified. All quantities in J are computed from $\rho_{\text{smooth}}(t)$.

B. Maximum Caliber Interpretation of the Weight

The time-local weight $w(t) = \text{Tr}[E(t)\,\rho(t)]$ admits a Maximum Caliber interpretation. MaxCal assigns probabilities to trajectories by maximizing path entropy subject to dynamical and boundary constraints. Imposing the terminal constraint that the experiment ends in outcome F reweights the unconditioned trajectory ensemble:

$$\mathcal{P}[\gamma \mid F] \propto \mathcal{P}_0[\gamma]\,\text{Tr}[F\,\rho_\gamma(t_f)]. \tag{8}$$

Using the duality $\text{Tr}[A\Phi(B)] = \text{Tr}[\Phi^\dagger(A)B]$ and the backward evolution $E(t) = \Phi^\dagger_{t_f\leftarrow t}(F)$, the reweighting factor at intermediate time t is precisely $\text{Tr}[E(t)\,\rho(t)] = w(t)$.

Thus the PQS weight coincides with the MaxCal trajectory reweighting under terminal constraints. The rigorous justification comes from PQS and quantum smoothing theory; MaxCal provides an interpretive framework connecting two-time conditioning to path-entropy maximization.

C. TSVF Weak Values and Weight Consistency

For unitary, pure-state evolution with initial state $|\psi_0\rangle$ and terminal postselection onto $|\phi\rangle$, the PQS conditioned expectation of an observable A reduces to the standard Two-State Vector Formalism (TSVF) result. The PQS expression

$$\langle A\rangle_{\text{PQS}}(t) = \frac{\text{Tr}\big[A\,\rho(t)\,E(t)\big]}{w(t)} \tag{9}$$

becomes the weak value $\langle A\rangle_{\text{weak}} = \text{Re}\,\frac{\langle\phi(t)|A|\psi(t)\rangle}{\langle\phi(t)|\psi(t)\rangle}$ when $\rho = |\psi\rangle\langle\psi|$ and $E = |\phi\rangle\langle\phi|$. The weight $w(t) = \text{Tr}[E(t)\rho(t)] = |\,\langle\phi(t)|\psi(t)\rangle\,|^2$ is precisely the TSVF normalization. This consistency confirms that our entropy-throughput construction uses the canonical two-time conditioning.

D. No-Signaling Proof

Two-boundary conditioning preserves no-signaling. For an early measurement with outcomes a and a later POVM $\{F_b\}$, the marginal $p(a|x) = \sum_b p(a,b|x)$ is independent of the POVM choice because $\sum_b F_b = \mathbb{1}$ and forward evolution is trace-preserving. The backward effect $E(t)$ is a retrodiction tool (it requires post-selection on future outcomes and cannot be known before time t), not a physical signal [14].

E. Numerical Protocols

For small systems ($n = 2, 3$) we exponentiate the Lindblad generator $\mathcal{L}$ as a matrix in Liouville space. For larger chains ($n = 3$–8), we implement the Liouvillian action directly on density-matrix elements using bit operations and integrate with RK4. The PQS entropy rate is computed by centered finite differences of the relative entropy. The Liouvillian spectral gap Δ is computed directly via sparse eigenvalue methods (shift-invert mode targeting eigenvalues near zero) for $n = 3, 5, 7$.

Default parameters: $T = 4.0$, $N = 200$, $\gamma = 0.1$, $\theta_2 = 0.5$. Robustness is verified by varying (T, N) and confirming stability of $J(\lambda)$, $\chi(\lambda)$, and λ_c. Code: `github.com/MiguelDelao/q-crit`.

F. Additional robustness data

Figure 7: varying (T, N) leaves $J(\lambda)$ and the susceptibility peak unchanged. Figure 8: varying initial states and terminal POVMs reshapes the detailed curves but preserves the crossover band. Figure 9: alternative coherence measures (ℓ_1, relative-entropy) produce balance points in the same region, confirming metric-independence of the critical window.

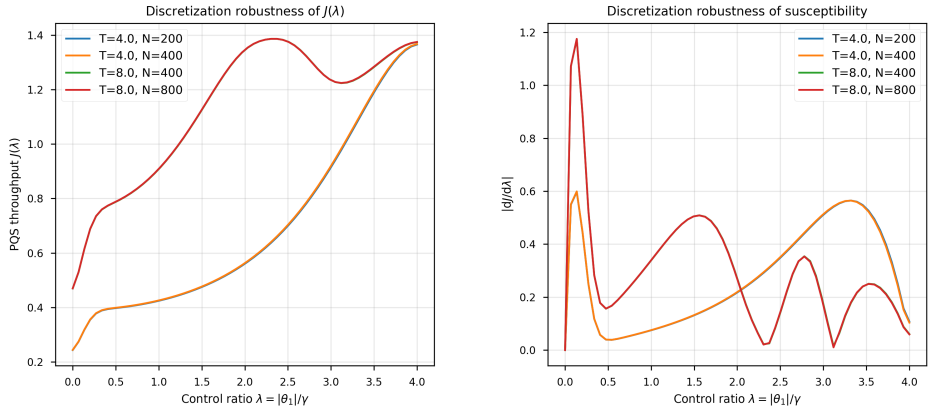

Figure 7: **Discretization robustness.** PQS throughput $J(\lambda)$ and the associated susceptibility $|\mathrm{d}J/\mathrm{d}\lambda|$ for several choices of total time T and number of time steps N. The curves and the inferred crossover location λ_c remain stable across the tested discretizations.

G. Three-qubit chain model

A three-qubit XX+ZZ chain with Hamiltonian $H = \theta(\sigma_x^{(1)}\sigma_x^{(2)} + \sigma_x^{(2)}\sigma_x^{(3)} + \sigma_z^{(1)}\sigma_z^{(2)} + \sigma_z^{(2)}\sigma_z^{(3)})$ and local dephasing rate γ exhibits identical phenomenology (Fig. 10): sharp crossover in $J(\lambda)$, susceptibility peak at $\Gamma_{\mathrm{coh}} \approx \Gamma_{\mathrm{dec}} = 3\gamma$. The critical-throughput regime is generic.

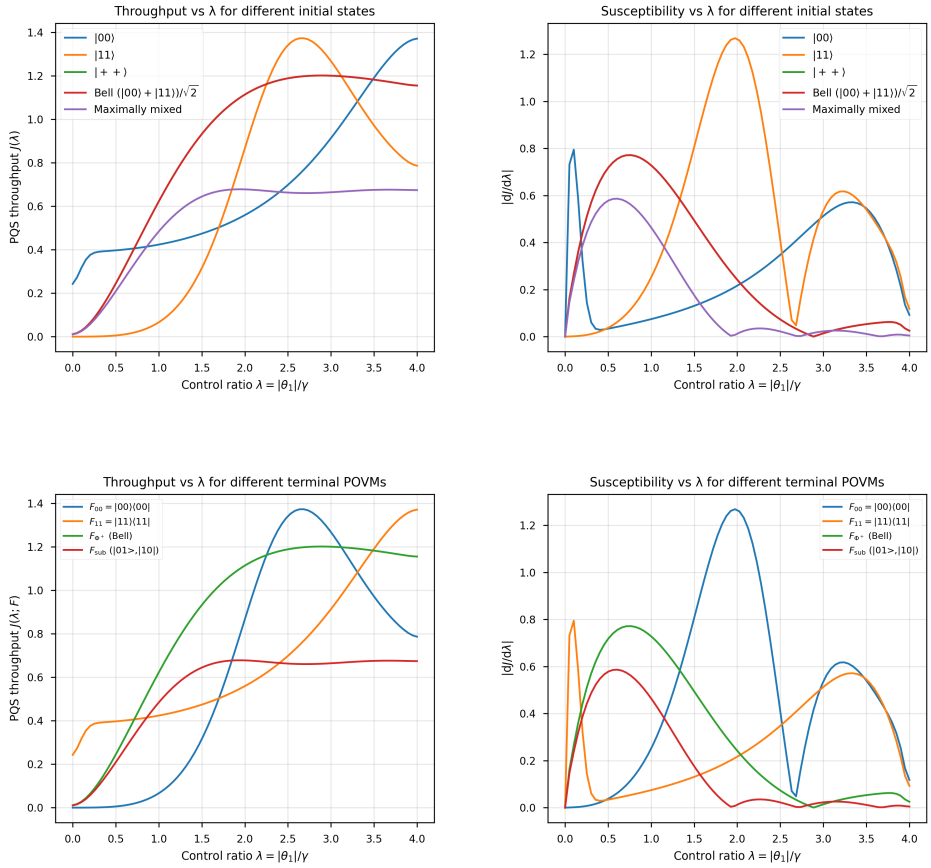

Figure 8: **Dependence on preparation and terminal POVM.** Top: PQS throughput $J(\lambda)$ and susceptibility for different initial states, including product states, Bell states, and the maximally mixed state. Bottom: the same quantities for different terminal POVM elements F. In all cases the detailed shape of $J(\lambda; F)$ changes, but a common crossover band separates a low-throughput regime from a saturated high-throughput regime.

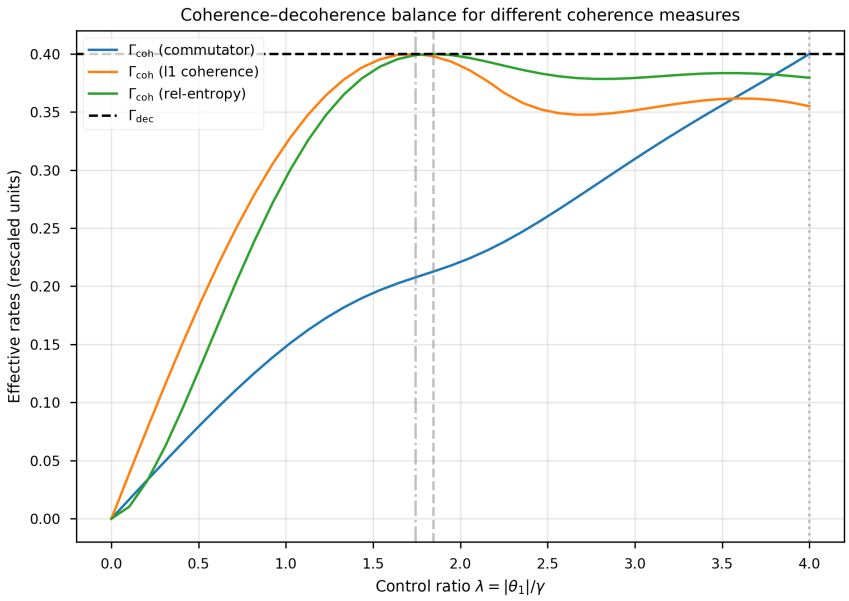

Figure 9: **Coherence-decoherence balance: comparison of coherence measures.** Effective coherence rates defined via a commutator norm, ℓ_1-coherence, and relative-entropy coherence, rescaled to allow comparison with the fixed decoherence rate $\Gamma_{\text{dec}} = 2\gamma$. All three measures identify a coherence-decoherence balance window in the same intermediate range of λ, supporting the metric-independence of the crossover.

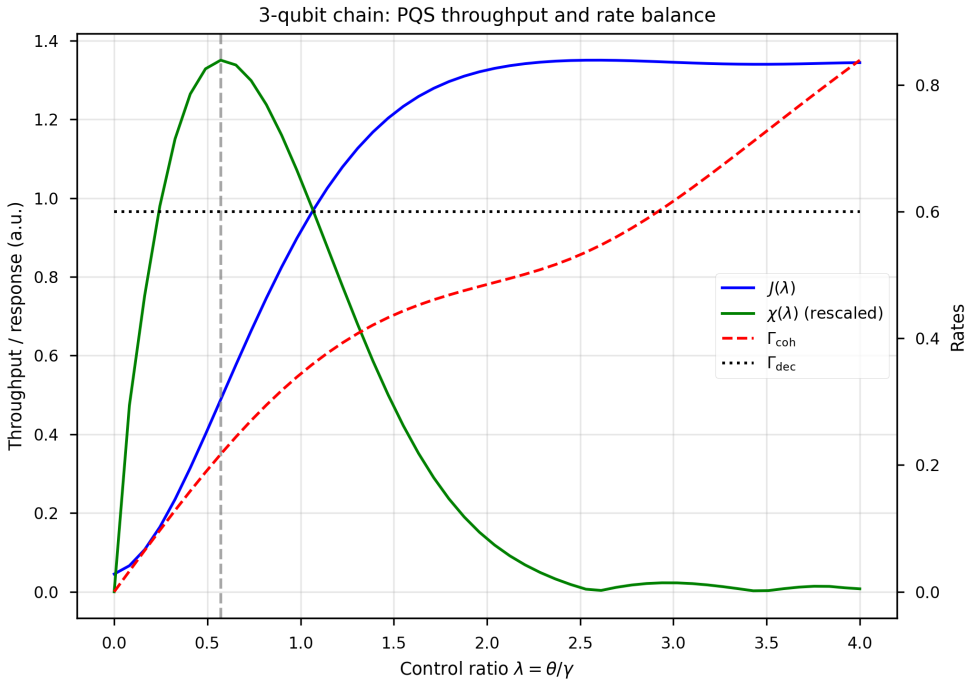

Figure 10: **Three-qubit chain results: PQS throughput and rate balance.** Entropy throughput $J(\lambda)$, susceptibility (rescaled), and coherence/decoherence rates for a three-qubit XX+ZZ chain with local dephasing. As in the two-qubit model, a pronounced susceptibility peak and a high-throughput crossover occur near the point where the coherence and decoherence rates balance.

References

[1] C. Maes, *Frenesy: Time-symmetric dynamical activity in nonequilibria*, Phys. Rep. **850**, 1 (2020).

[2] J. P. Garrahan and I. Lesanovsky, *Thermodynamics of Quantum Jump Trajectories*, Phys. Rev. Lett. **104**, 160601 (2010).

[3] A. B. Nascimento and L. C. Céleri, *Speedup of thermodynamic entropy production via quantum dynamical criticality*, Phys. Rev. A **110**, 052223 (2024).

[4] Google Quantum AI, *Measurement-induced entanglement and teleportation on a noisy quantum processor*, Nature **622**, 481 (2023).

[5] P. Strasberg and A. Winter, *First and Second Law of Quantum Thermodynamics: A Consistent Derivation Based on a Microscopic Definition of Entropy*, PRX Quantum **2**, 030202 (2021).

[6] R. Nigmatullin and M. Prokopenko, *Thermodynamic Efficiency of Interactions in Self-Organizing Systems*, Entropy **23**(6), 757 (2021).

[7] F. Carollo and I. Lesanovsky, *Stochastic thermodynamics at the quantum-classical boundary*, arXiv:2404.10118 (2024).

[8] G. Squillante, X. Turkeshi, M. Dalmonte, and D. Rossini, *Grüneisen parameter as an entanglement compass and the breakdown of the Hellmann-Feynman theorem*, Phys. Rev. B **108**, L140403 (2023).

[9] M. J. Gullans and D. A. Huse, *Dynamical purification phase transition induced by quantum measurements*, Phys. Rev. X **10**, 041020 (2020).

[10] M. Ippoliti *et al.*, *Entanglement phase transitions in measurement-only dynamics*, Phys. Rev. X **11**, 011030 (2021).

[11] H. Spohn, *Entropy production for quantum dynamical semigroups*, J. Math. Phys. **19**, 1227 (1978).

[12] S. Gammelmark, B. Julsgaard, and K. Mølmer, *Past Quantum States of a Monitored System*, Phys. Rev. Lett. **111**, 160401 (2013).

[13] M. Tsang, *Time-symmetric quantum theory of smoothing*, Phys. Rev. Lett. **102**, 250403 (2009).

[14] M. F. Pusey and M. S. Leifer, *Logical pre- and post-selection paradoxes are proofs of contextuality*, arXiv:1506.07850 (2015).

[15] X.-C. Zhuang, S.-H. Su, D. Wang, X.-M. Lu, J.-H. Eberly, and A. Miranowicz, *Identifying contributions of classical and quantum correlations to entropy production in non-equilibrium quantum processes*, Quantum Sci. Technol. **10**, 035065 (2025).

[16] S. M. Barnett, D. T. Pegg, and J. Jeffers, *Bayes' theorem and quantum retrodiction*, J. Mod. Opt. **47**, 1779 (2000).

[17] J. P. Santos, L. C. Céleri, G. T. Landi, and M. Paternostro, *The role of quantum coherence in non-equilibrium entropy production*, npj Quantum Inf. **5**, 23 (2019).

[18] A. A. Abbott, C. Giarmatzi, F. Costa, and C. Branciard, *Multi-time measurements in quantum mechanics*, Phys. Rev. A **94**, 032131 (2016).